



Photocatalytic behavior of ZnO and Pt-incorporated ZnO nanoparticles in phenol degradation

N. Morales-Flores, U. Pal*, E. Sánchez Mora

Instituto de Física, Benemérita Universidad Autónoma de Puebla, 18 Sur y Av. San Claudio, Puebla, Pue. 72570, Mexico

ARTICLE INFO

Article history:

Received 10 October 2010

Received in revised form 5 January 2011

Accepted 6 January 2011

Available online 12 January 2011

Keywords:

Photocatalysis

Phenol degradation

ZnO

Pt–ZnO

HPCL

ABSTRACT

Nanostructured Pt–ZnO composite thick films were prepared using the composite nanoparticles synthesized through Triton X-100 polymer assisted thermolysis of zinc acetate. It has been observed that only a fraction of added Pt incorporates into the ZnO lattice and the rest segregates over the ZnO nanoparticle surface to form metallic nanoclusters. Morphology, crystallinity, and optical properties of the ZnO and Pt–ZnO nanostructures have been studied. Photocatalytic behavior of the samples for phenol degradation process has been studied in a high performance liquid chromatography system. It has been observed that though the phenol degradation rate is higher for pure ZnO nanostructures, Pt–ZnO nanostructures act as selective catalyst, producing only one intermediate product and dissociating it faster than ZnO.

© 2011 Elsevier B.V. All rights reserved.

1. Introduction

Metal oxide catalysts are widely used in chemical processes for selective oxidation, total oxidation, hydrogenation, and environmental applications. Among them, selective oxidation through heterogeneous catalysis is the most typical example of the use of metal oxide catalysts [1]. Several semiconductors have been utilized for photocatalytic degradation of environmentally benign organic compounds [2–6]. Among them, most extensively studied is the titanium dioxide (TiO₂). On the other hand, recently zinc oxide (ZnO) with band gap energy (3.37 eV at room temperature) similar to TiO₂ has attracted much attention for its photocatalytic applications owing to its high photosensitivity and thermal stability [7–9]. Though TiO₂ has been a preferred material for photocatalytic applications due to its suitable band gap energy (3.0–3.32 eV, depending on crystalline structure), high thermal stability and non-toxicity [10–12], in spite of having similar band gap energy and high absorption efficiency for a large fraction of solar spectrum than TiO₂, ZnO has not been thoroughly investigated as catalyst [13]. A semiconductor suitable for photocatalysis has to be (i) photoactive, (ii) able to use visible or near-UV light, (iii) biologically and chemically inert, (iv) photo-stable, and (v) of reasonably low cost [14]. Of the common semiconductors, zinc oxide (ZnO) is the one that fulfills all the previous conditions. In nanostructure forms, both of these oxide semiconductors (TiO₂ and ZnO) should work as bet-

ter catalysts/photocatalysts due to their high specific surface areas [15].

Usually, the properties of nanomaterials depend on their size, morphology, and dimensionality. Semiconductor nanostructure catalysts have been utilized traditionally not only to produce useful chemicals [16], but also to convert pollutants in waste streams to innocuous or less harmful form [17–19]. Heterogeneous photocatalysis is an advanced oxidation process (AOP), which generates hydroxyl radicals ($\cdot\text{OH}$) by oxidation of adsorbed OH[−] or H₂O molecules on a semiconductor surface while it is irradiated with light of energy greater than its band gap [20]. The $\cdot\text{OH}$ radicals are extremely powerful oxidants, being able to degrade a great variety of organic compounds [21].

Kawaguchi and Uejima have studied the photocatalytic decomposition of phenol in aqueous suspensions of ZnO [22]. They observed that the photo-reactivity decreases with increasing initial concentration of phenol and the rate of chemical oxygen demand (COD) reduction is much slower than that of phenol decomposition. Okamoto et al. have studied the heterogeneous photocatalytic decomposition of phenol over TiO₂ powder [12], confirming that the hydroxyl radicals are the true reactive species which are formed not only via holes generated on illuminated semiconductors but also via H₂O₂ generated from O₂^{•−}. Pardeshi and Patil [23] have studied the photodegradation of phenol in aqueous ZnO suspensions under solar irradiation and found the degradation process is more effective under solar light in comparison to artificial visible light irradiation. However, their used ZnO samples were commercial (Merck, Specialities Pvt. Ltd., Mumbai) and the sizes of the particles were not specified. On the other hand, very recently Hayat

* Corresponding author. Fax: +52 222 2295611.

E-mail address: upal@sirio.ifuap.buap.mx (U. Pal).

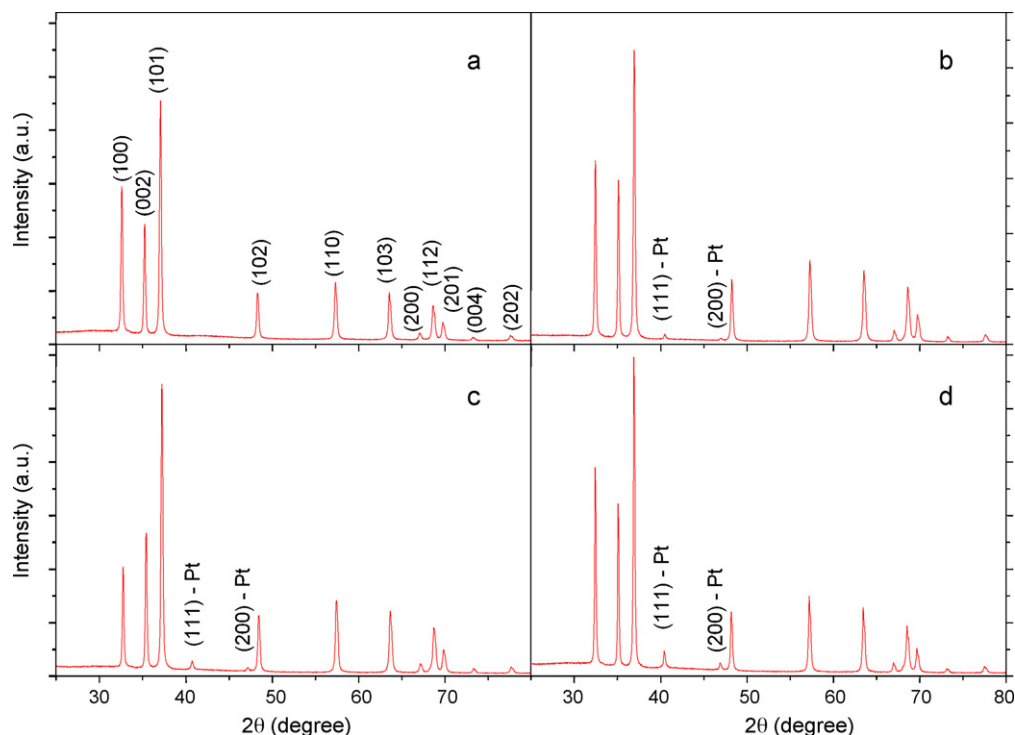


Fig. 1. XRD patterns of ZnO nanostructures: (a) ZnO, (b) Pt–ZnO 0.5%, (c) Pt–ZnO 1.0%, and (d) Pt–ZnO 2.0% (nominal). The arrows indicate the diffraction peaks attributed to metallic Pt phase.

et al. [24] have applied sol–gel derived ZnO nanoparticles for phenol degradation under UV laser irradiation and found the nanoparticles annealed at 500 °C were most active catalysts for that purpose with degradation rate constant of 0.0391 min⁻¹. High photocatalytic activity of the ZnO nanoparticles was attributed to their smaller particle size and better dispersion.

Phenols are the primary chemicals and also the residues of chemical wastes/byproducts of many industries, such as paper mills, herbicide and fungicide production plants, etc. [25]. Photocatalysis has been proven to be a plausible technique to decontaminate phenolic waste-water as complete mineralization has been successfully achieved under a variety of conditions [26,27].

In the present article, we report on the photocatalytic decomposition behavior of phenol on ZnO nanoparticles and Pt–ZnO composite nanoparticles. The ZnO and Pt–ZnO nanoparticles with different Pt contents were fabricated through a low cost Triton X-100 polymer assisted technique. The nanostructures were characterized by scanning electron microscopy (SEM), X-ray diffraction (XRD), transmission electron microscopy (TEM), UV–Vis optical absorption, diffuse reflectance spectroscopy (DRS) and Raman spectroscopy techniques. Near room temperature photo-degradation of phenol and its intermediate products were monitored by high performance liquid chromatography (HPLC).

2. Experimental

ZnO nanoparticles and Pt–ZnO composite nanoparticles were synthesized through Triton X-100 polymer assisted thermolysis of zinc acetate [(CH₃COO)₂Zn]. Briefly, appropriate amounts of zinc acetate dihydrate [Zn(CH₃COO)₂·2H₂O, Baker, 99.9%] were dissolved in 15 ml of deionized water under vigorous stirring. Then about 5.8 ml of Triton X-100 [(C₂H₄O)_nC₁₄H₂₂O, Aldrich] was slowly added into the mixture solution. After 2 h of aging under magnetic stirring, the mixture solution was introduced into a muffle furnace, and heated at 250 °C for 36 h. The dry product was then

calcinated at 550 °C for 2 h in a tubular furnace under air ambient. Structure, crystallinity, and morphology of the final product were analyzed using Phillips X'Pert X-ray diffractometer, a Horiba Jovin-Yvon, LabRAM HR micro-Raman system, and a JEOL JSM-5600LV scanning electron microscope attached with Noran Super Dry analytical system, respectively. For studying the optical and microstructural characteristics of the nanostructures, a Varian Cary 100 UV–Vis spectrophotometer with DRACA-30I diffuse reflectance accessory, and a JEOL 2010F transmission electron microscope were utilized.

On the other hand, for preparing 2-D films structure of the samples, first an aqueous solution of acetic acid [CH₃COOH] (0.1 ml of acetic acid in 50 ml of deionized water) was prepared. Then about 500 mg of ZnO or Pt–ZnO sample (powder) was mixed homogeneously with 0.5 ml of Triton X-100 polymer. About 0.5 ml of the previously prepared acetic acid solution was added to the latter mixture. The homogenized colloidal mixture was then dispersed over well cleaned glass substrates and drawn by another glass substrate to make continuous and uniform layers. Finally, the nanostructured films were thermally treated at 550 °C for 5 h in air ambient. Thicknesses of the prepared films were measured using a Veeco Dektak 150 profilometer, which varied in between 50 and 60 μm. All the samples in thick film form were characterized by SEM, XRD, TEM, DRS, and room temperature micro-Raman spectroscopy (with 632.82 nm line of a He–Ne laser as excitation source) techniques.

A Perkin-Elmer Series 200 HPLC system was utilized for monitoring the photocatalytic behavior of the nanostructures. The photochemical reactor used in the present study consisted of a Pyrex glass. The photo-degradation rate of phenol in water was monitored dispersing solid catalyst and under oxygen flow to trap electrons. Cold water was circulated in the annulus of the reactor to maintain the solution temperature below 22 °C, as excess temperature could deplete the dissolved oxygen in the solution. The source light was placed concentrically over the pyrex glass container filled with 4 ml of the aqueous reaction mixture and fed into the vessel to

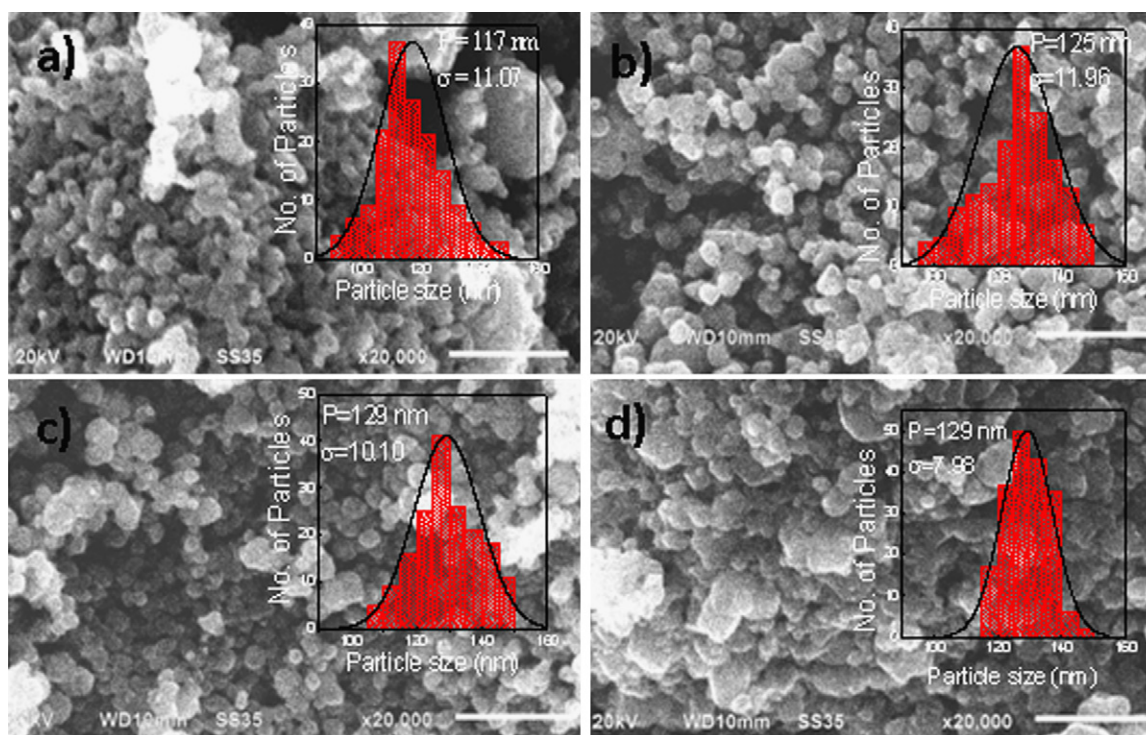


Fig. 2. Typical SEM micrographs and size distribution histograms (insets) of the ZnO nanoparticles: (a) ZnO, (b) Pt–ZnO 0.5%, (c) Pt–ZnO 1.0%, and (d) Pt–ZnO 2.0% (nominal).

be degraded. The concentration of phenol in the mixture solution was 15 ppm. The catalyst containing reaction mixture was illuminated by a mercury ultraviolet lamp (Upland, model XX-15S). The lamp radiated predominantly at $\lambda = 254$ nm with an intensity of $1600 \mu\text{W}/\text{cm}^2$. The distance between the UV light source and the reaction solution was about 15 cm. A series of batch experiments was conducted at different running time (15, 30, 45, 60, 120 min).

The concentrations of phenol and the intermediate products formed during its degradation were quantitatively analyzed through the HPLC system. The HPLC system consisted of an isocratic pump, injector, a C-18 column, a diode-array as UV–Vis detector, and a computer controlled data acquisition system. The mobile phase consisted of an acetonitrile–water mixture at 60:40 volumetric ratio. The analysis conditions were 1.0 ml/min liquid flow rate, temperature = 25°C , detecting/monitoring wavelength $\lambda = 280$ nm. The chromatographic areas of phenol were converted to concentration values using the calibration curves.

3. Results and discussion

Fig. 1 shows the XRD patterns of the ZnO and Pt–ZnO nanostructured films. The XRD patterns of Pt–ZnO composites reveal the presence of wurtzite ZnO (JCPDS Card No. 36-1451) as major phase. In general, the intensity of XRD peaks attributed to wurtzite ZnO increased with the increase of Pt content in the samples. On the other hand, there appeared two distinct peaks related to metallic Pt, the intensity of which increased with the increase of Pt concentration (nominal) in the samples. There appeared no significant shift of position for the main diffraction peaks related to ZnO on incorporating Pt in the samples, indicating only a minor portion of the added Pt was incorporated into the ZnO lattice.

Fig. 2 shows the typical SEM images of the ZnO and Pt–ZnO films. As can be seen, all the samples consist of spherical shaped nanoparticles with mean diameter ~ 120 nm. While the increase of nominal Pt concentration increased the Pt content in the samples as revealed from their energy dispersed X-ray (EDX) analysis (Table 1), it did not induce any significant change either in the morphology

Table 1

EDS composition analysis of the ZnO and Pt–ZnO nanoparticles.

Sample	Composition (atom %)		
	Pt	Zn	O
ZnO	0	50.91	49.09
Pt–ZnO 0.5%	0.04	50.33	49.63
Pt–ZnO 1.0%	0.14	50.71	49.15
Pt–ZnO 2.0%	0.27	50.68	49.05

or in the size of the nanoparticles. In fact, most of the added Pt segregated from the interior of the nanoparticles to form small Pt clusters at the surface, as can be seen from the typical TEM image of the Pt–ZnO sample presented in Fig. 3. The bright contrast clusters in between 1.5 and 3.0 nm size range dispersed over the surface of the ZnO nanoparticles must be of Pt as the atomic number of

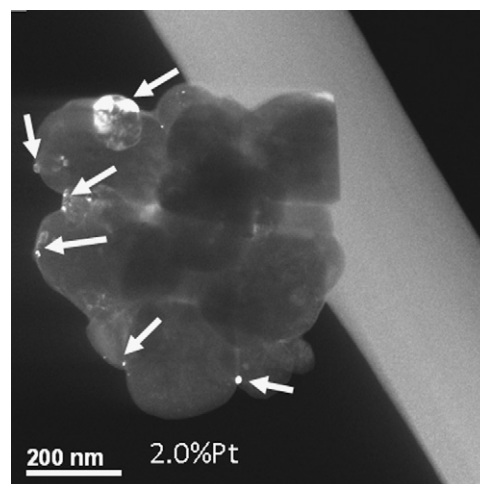


Fig. 3. A typical dark-field TEM image of the Pt–ZnO 2.0% nanoparticles. The arrows indicate formation of metallic Pt nanoparticles over the ZnO particle surface.

metallic Pt is much higher than the average atomic number of zinc and oxygen. Sun et al. [28] have also observed the formation of Pt clusters over the surface of TiO₂ (Degusa P25) nanoparticles in their Pt–TiO₂ composite samples when the concentration of incorporated Pt was high. Lee and Tu have also observed the segregation of Pt over the surface of nanostructured ZnO thin films when prepared by electrodeposition [29] and associated the phenomenon to the high surface energy of Pt (2.691 J m⁻² at 298.2 K). However, as indicated by the XRD patterns of the composite samples, a small fraction of the added Pt could be incorporated into the ZnO lattice sites, substituting zinc atoms (ionic radius of Zn, O and Pt are 0.74, 1.40, and 0.96 Å, respectively).

Optical absorption spectra of the ZnO and Pt–ZnO samples in the UV–Vis spectral range are shown in Fig. 4a. All the spectra revealed sharp absorption edge at about 375 nm, characteristic of crystalline ZnO. However, with the increase of Pt content, the intensity of their absorption tails at higher wavelength side increased, which might be due to the presence of Pt clusters over the surface of ZnO nanoparticles, making them more dispersive. The change in the dispersive nature of the samples was also manifested from their color (the color changed from white to gray on increasing the Pt content), which could be perceived by naked eye. Similar optical behavior of the samples was also revealed in their diffused reflectance spectra (Fig. 4b). While absorption edge did not change noticeably, the reflectance value decreased with the increase of Pt content in the composite samples.

The diffused reflectance spectra of the samples after Kubelka–Munk (KM) transformation are shown in Fig. 5. The band gap energy of the samples was estimated from the intersection between the linear fit of the KM function and the energy axis [30]. As can be seen from Fig. 5, there is no significant influence of the incorporated platinum on the band gap energy (E_g) value of the ZnO nanoparticles.

Fig. 6 shows the Raman spectra of the ZnO and Pt–ZnO samples. The Raman spectrum of ZnO sample revealed eight peaks, located at about 100, 207, 327, 416, 437, 504, 560 and 663 cm⁻¹. The peak centered at about 100 cm⁻¹ is attributed to E_{2L} mode. The peaks at 416, 437 and 560 cm⁻¹ are attributed to the E_{1T} , E_{2H} and LO modes of wurtzite ZnO, respectively. The peaks centered at about 207 and 327 cm⁻¹ have been previously observed in ZnO by several authors [31–35] and were attributed to the second order modes or multi-phonon processes. The peak at 504 cm⁻¹ is attributed to 2- B_{2L} silent

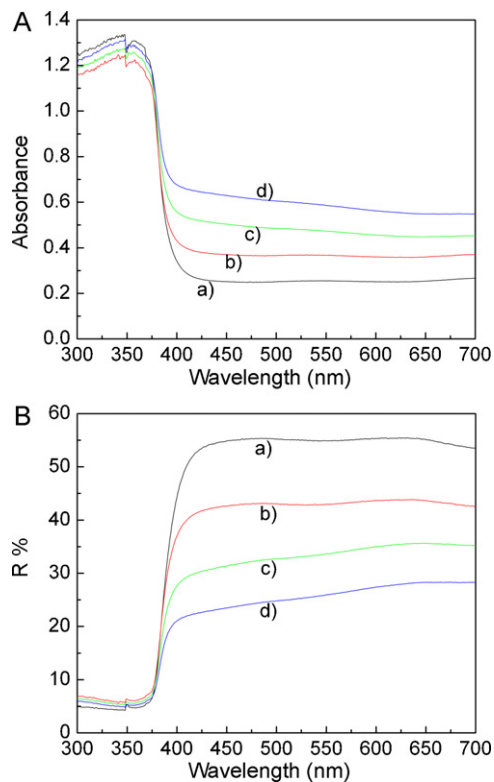


Fig. 4. (A) UV–Vis absorption spectra and (B) diffuse reflectance spectra of the ZnO nanostructures: (a) ZnO, (b) Pt–ZnO 0.5%, (c) Pt–ZnO 1.0%, and (d) Pt–ZnO 2.0% (nominal).

mode [36] and the peak located at 663 cm⁻¹ is attributed to TA + LO mode in the ZnO [37,38]. In the Pt–ZnO samples, the E_{2H} Raman peak associated to oxygen sub-lattice of ZnO become broader and less intense with the incorporation of Pt, which might be associated to the disorder produced in the ZnO lattice by Pt incorporation.

3.1. Photocatalytic activity

As the adsorption of phenol takes place over the ZnO film surface even before UV irradiation [39], the catalyst was equilibrated

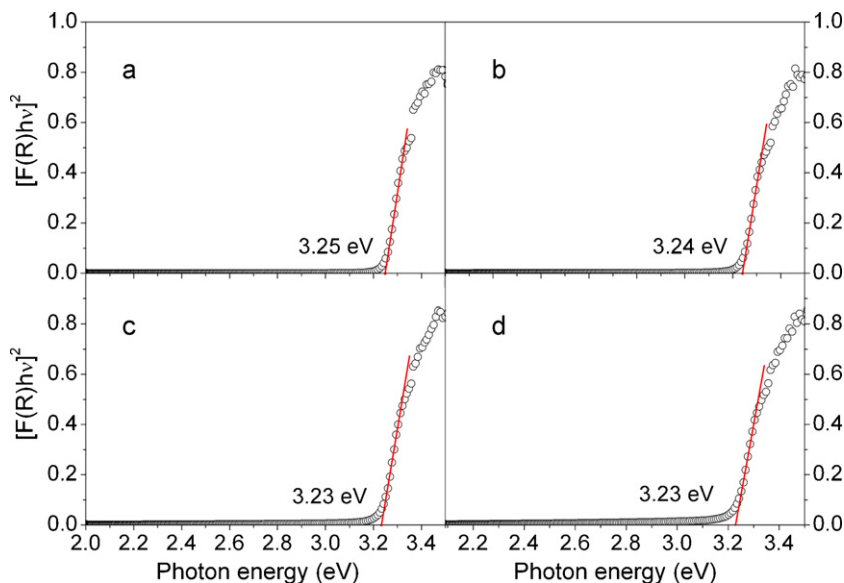


Fig. 5. Kubelka–Munk transformed reflectance spectra of ZnO nanostructures: (a) ZnO, (b) Pt–ZnO 0.5%, (c) Pt–ZnO 1.0%, and (d) Pt–ZnO 2.0% (nominal).

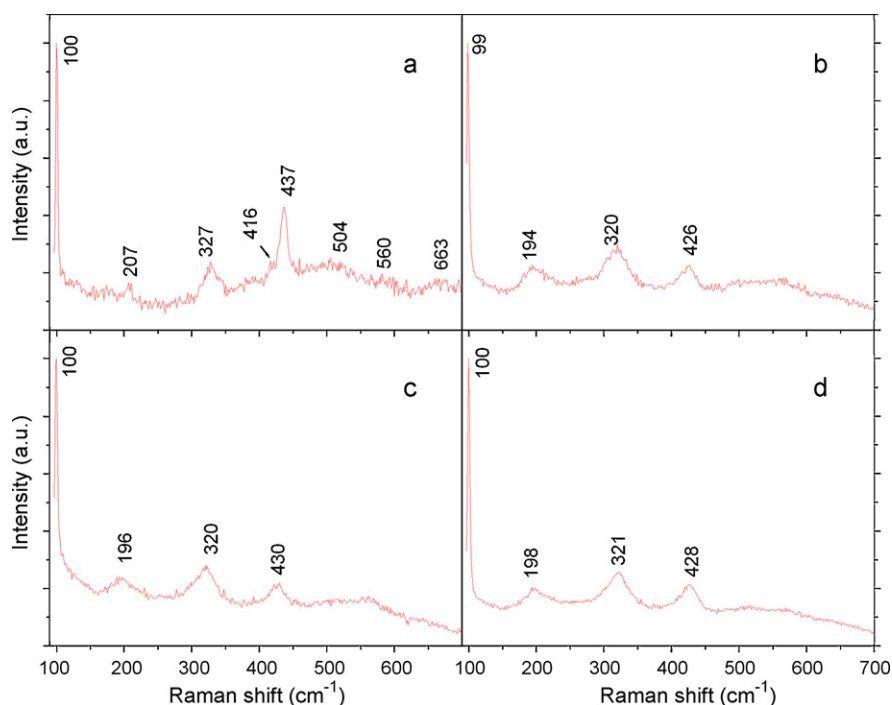


Fig. 6. Raman spectra of ZnO nanostructures: (a) ZnO, (b) Pt–ZnO 0.5%, (c) Pt–ZnO 1.0%, and (d) Pt–ZnO 2.0% (nominal).

in reaction solution under dark for about 60 min. Fig. 7a shows the chromatograms of phenol solution under UV irradiation in contact with ZnO film. From the figure, we can see the retention time of phenol is about 1.4 min. The retention time was measured as the

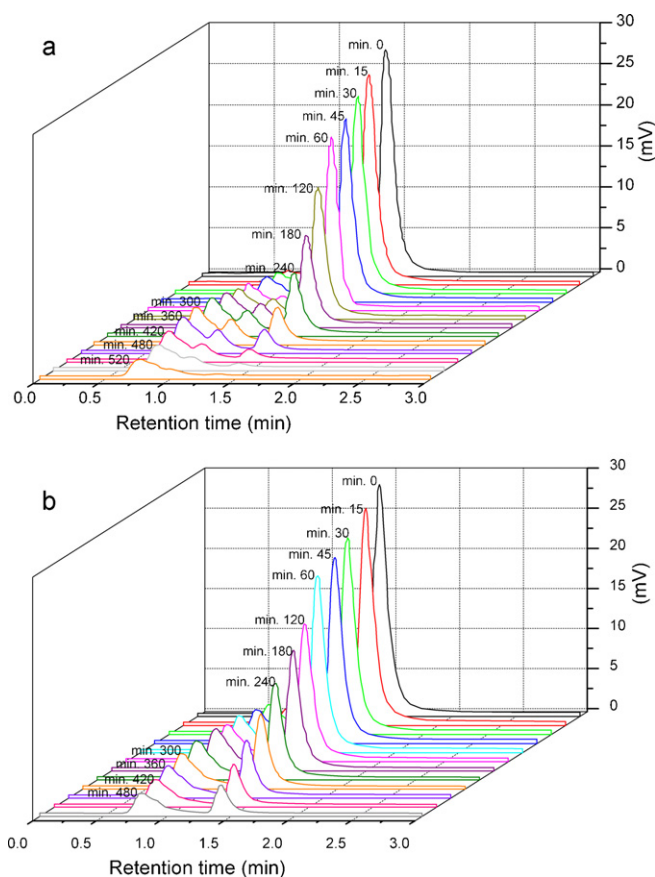


Fig. 7. Chromatograms of the (a) pure ZnO and (b) Pt–ZnO (2.0% nominal) catalyst at different running times.

interval between the times of sample injection and the time when the chromatogram reveals maximum peak height for phenol. After 15 min of UV irradiation, the peak intensity corresponding to phenol decreased and there appeared two peaks at retention times of 0.8 and 1.0 min, which correspond to the formation of hydroquinone and catechol, respectively [40]. The peak correspond to phenol almost disappeared approximately at 540 min of UV irradiation, indicating its total degradation. During phenol degradation, hydroquinone is formed as the major product and catechol is produced as minor product (Fig. 8). On the other hand, for the sample containing 2.0% Pt (nominal) (Fig. 7b), apart from the peak correspond to phenol, there appeared only one peak (hydroquinone) at retention time of about 0.8 min. Unlike pure ZnO, no total degradation of phenol was possible up to 540 min of UV irradiation for the Pt–ZnO sample. Details analysis of the evolution of intermediate products and their dissociation are presented in Fig. 9.

For comparison, the results of photocatalytic degradation of phenol by pure ZnO and Pt incorporated ZnO nanoparticles are presented in Fig. 10. As can be seen, pure or undoped ZnO nanoparticles have better photocatalytic activity than the composite Pt–ZnO nanoparticles. The photocatalytic efficiency of the Pt–ZnO samples decreased gradually with the increase of platinum concentration.

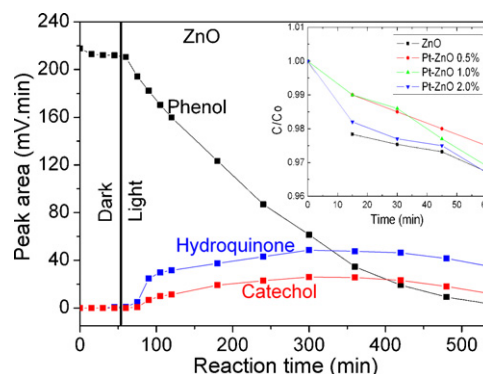


Fig. 8. Adsorption and photo-degradation rate of phenol over ZnO nanoparticles.

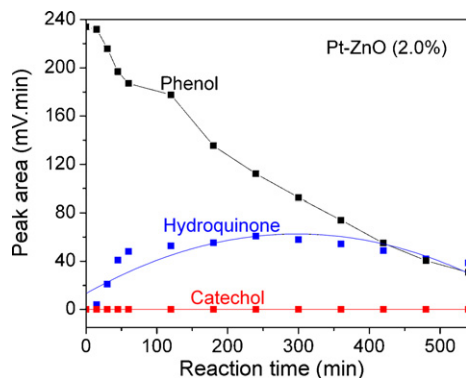


Fig. 9. Adsorption and photo-degradation rate of phenol over Pt-ZnO (2.0% nominal) nanoparticles.

As has been mentioned earlier, such a reduction in photocatalytic activity can be attributed to the formation of Pt clusters on the surface of ZnO particles. Similar observation has also been made by Lee and Tu [29] for the Pt incorporated ZnO thin films prepared by electrodeposition.

Sun et al. [28] have studied the photocatalytic oxidation of phenol on TiO₂, and noticed that the platinum can decrease the activity of TiO₂ in photocatalytic oxidation, possibly due to water reduction over the surface of platinum particles, that cannot take place on pure TiO₂. Water reduction to hydrogen will consume a part of photo-generated electrons that otherwise could take part in oxygen reduction, forming reactive oxygen species. Though the Pt-ZnO interface can transfer electrons from ZnO to Pt metal through charge equilibrium process [41], decreasing electron-hole recombination process to enhance photocatalytic activity, formation of Pt cluster over the surface of ZnO nanoparticles effectively reduces the contact area between the phenol solution and ZnO particles. We believe, this reduction of active surface area, along with the partial consumption of photo-generated electrons for water reduction process reduces the photocatalytic activity of our Pt-ZnO composite samples. However, the kinetic parameters of the phenol photocatalytic degradation process of our samples indicate that, though the formation of Pt clusters over the surface of ZnO nanoparticles cannot increase the phenol degradation rate, it increases the rate of decomposition of the intermediate products. Moreover, the Pt-ZnO catalysts are selective, as they produce only one intermediate product (Figs. 11 and 12).

3.2. Mechanism of photocatalytic reaction

A mechanism of the photocatalytic action of semiconductors is somewhat more complicated [42]. The photo-degradation mech-

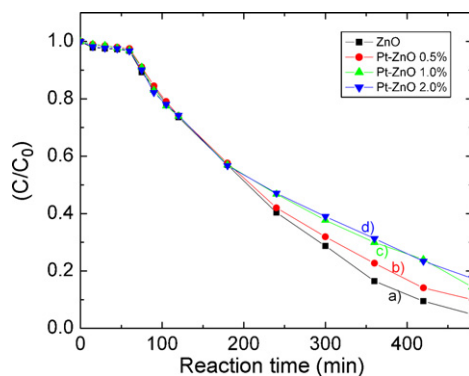


Fig. 10. Phenol photo-degradation rate of ZnO nanoparticles: (a) ZnO, (b) Pt-ZnO 0.5%, (c) Pt-ZnO 1.0%, and (d) Pt-ZnO 2.0% (nominal).

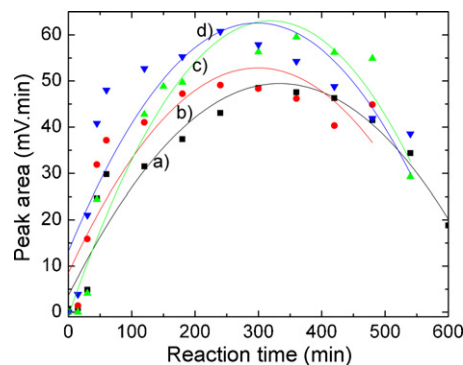
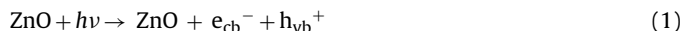


Fig. 11. Formation and degradation rate of hydroquinone as intermediate product by: (a) ZnO, (b) Pt-ZnO 0.5%, (c) Pt-ZnO 1.0%, and (d) Pt-ZnO 2.0% (nominal) catalysts.

anism of phenol by ZnO could be similar to that of TiO₂, which has been reported by several authors [40,43–46]. When the photocatalyst ZnO is irradiated with ultraviolet (UV) radiation from sunlight or other illuminated light source (e.g. fluorescent lamps), it produces electron-hole pairs on or near the surface (Eq. (1)) through electron transfer from the valence band to the conduction band across the band gap of the semiconductor. This state is referred as the semiconductor's photo-excitation state. The electron-hole pair quickly diffuses to the surface. These photo-generated electron-hole pairs can recombine within a time scale of nanoseconds to radiate heat [10]. Such a short lifetime would not allow the electrons and holes to participate in any chemical reaction.



Therefore, the electrons and holes should be captured by any of chemical species which exist on the surface (ions, atoms, molecules, etc.), or by the so-called surface traps. Hydroxyl radicals are generated when the surface adsorbed water or hydroxyl anions react with the valence band hole of the UV excited ZnO (Eqs. (2) and (3)).



Superoxide radicals are generated by the interaction of atmospheric oxygen or dissolved oxygen of the reaction solution with the conduction band electrons of the UV excited ZnO (Eq. (4)):



Hydroxyl radicals could also be formed through an alternate route. Reaction of superoxide radical with H⁺ ions generates OH₂[•] (Eqs. (5))

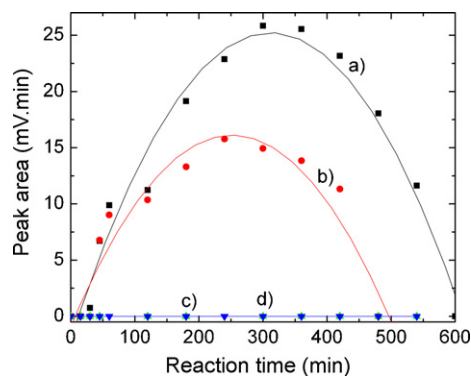
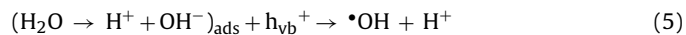


Fig. 12. Formation and degradation rate of catechol as intermediate product by: (a) ZnO, (b) Pt-ZnO 0.5%, (c) Pt-ZnO 1.0%, and (d) Pt-ZnO 2.0% (nominal) catalysts.

and (6)), which reacting with other similar species produces hydrogen peroxide (Eq. (7)). The produced hydrogen peroxide, reacting with conduction band electrons, generates more hydroxyl radicals (Eq. (8)):



Thus the hydroxyl and superoxide radicals attack the adsorbed phenolic compound to give hydroxylated and phenoxy intermediaries [41,43], yielding open ring fragments like linear chain carboxylic acids freeing the occupied ZnO sites; finally generating the final products. The cycle continues as long as illumination is continued, or the mineralization of the phenol is completed.

4. Conclusions

ZnO and Pt–ZnO composites nanoparticles could be synthesized at large scale and low cost through Triton X-100 polymer assisted method. All the nanoparticles were of spherical shape and uniform size, with mean diameter of about 120 nm. Only a small fraction of the added Pt gets incorporated into the ZnO lattice, and the rest remain dispersed over the surface of ZnO particles as metallic clusters. While ZnO nanoparticles could photodegrade phenol totally in 540 min, the process is slower for the case of Pt–ZnO nanoparticles. Though Pt incorporation into ZnO nanoparticles does not enhance the photodegradation rate of phenol, it produces only one intermediate product and decomposes the intermediate product very fast. Such a selective catalytic behavior of Pt–ZnO composite nanoparticles should be of utmost importance in the area of organic synthesis.

Acknowledgement

The work was partially supported by the VIEP, BUAP through 2010 project grant.

References

- [1] B.M. Weckhuysen, D.E. Keller, *Catal. Today* 78 (2003) 25–46.
- [2] D.W. Bahnemann, C. Kormann, M.R. Hoffmann, *J. Phys. Chem.* 91 (1987) 3789–3798.
- [3] F.L. Toma, G. Bertrand, D. Klein, C. Coddet, *Environ. Chem. Lett.* 2 (2004) 117–121.
- [4] B.C. Faust, M.R. Hoffmann, D.W. Bahnemann, *J. Phys. Chem.* 93 (1989) 6371–6381.
- [5] S.N. Frank, A.J. Bard, *J. Phys. Chem.* 81 (1977) 1484–1488.
- [6] D.F. Ollis, *Environ. Sci. Technol.* 19 (1985) 480–484.
- [7] A.J. Hoffman, E.R. Carraway, M.R. Hoffmann, *Environ. Sci. Technol.* 28 (1994) 776–785.
- [8] E.S. Jang, J.H. Won, S.J. Hwang, J.H. Choy, *Adv. Mater.* 18 (2006) 3309–3312.
- [9] T.J. Kuo, C.N. Lin, C.L. Kuo, M.H. Huang, *Chem. Mater.* 19 (2007) 5143–5147.
- [10] M.R. Hoffmann, S.T. Martin, W. Choi, D.W. Bahnemann, *Chem. Rev.* 95 (1995) 69–96.
- [11] P.H. Breen, B. Mazumdar, S.C. Skinner, R.F.P. Nogueira, W.F. Jardim, *Solar Energy* 56 (1996) 471–477.
- [12] K. Okamoto, Y. Yamamoto, H. Tanaka, M. Tanaka, A. Itaya, *Bull. Chem. Soc. Jpn.* 58 (1985) 2015–2022.
- [13] S. Sakthivel, B. Neppolian, M.V. Shankar, B. Arabindoo, M. Palanichamy, V. Murugesan, *Sol. Energy Mater. Sol. Cells* 77 (2003) 65–82.
- [14] A. Sobczykński, A. Dobosz, *Pol. J. Environ. Stud.* 10 (2001) 195–205.
- [15] Q. Wan, T.H. Wang, J.C. Zhao, *Appl. Phys. Lett.* 87 (2005) 083105-1–083105-3.
- [16] M.A. Fox, *Acc. Chem. Res.* 16 (1983) 314–321.
- [17] H. Yoneyama, Y. Yamashita, H. Tamura, *Nature* 282 (1979) 817–818.
- [18] K. Kogo, H. Yoneyama, H. Tamura, *J. Phys. Chem.* 84 (1980) 1705–1710.
- [19] A.L. Pruden, D.F. Ollis, *J. Catal.* 82 (1983) 404–417.
- [20] A.L. Linsebigler, G. Lu, J.T. Yates Jr., *Chem. Rev.* 95 (1995) 735–758.
- [21] J.-M. Herrmann, *Catal. Today* 53 (1999) 115–129.
- [22] H. Kawaguchi, T. Uejima, *Kagaku Kogaku Ronbun.* 9 (1983) 107–109.
- [23] S.K. Pardeshi, A.B. Patil, *Solar Energy* 82 (2008) 700–705.
- [24] K. Hayat, M.A. Gondal, M.M. Khaled, S. Ahmed, A.M. Shamsi, *Appl. Catal. A* (2010), doi:10.1016/j.apcata.2010.11.032.
- [25] C. Baird, *Environmental Chemistry*, Freeman, New York, 1998.
- [26] N. Serpone, R. Terzian, C. Minero, E. Pelizzetti, *J. Am. Chem. Soc.* 238 (1993) 281–314.
- [27] J.C. D'Oliveira, G. Al-Sayyed, P. Pichat, *Environ. Sci. Technol.* 24 (1990) 990–996.
- [28] B. Sun, A.V. Vorontsov, P.G. Smirniotis, *Langmuir* 19 (2003) 3151–3156.
- [29] M.-K. Lee, H.-F. Tu, *J. Electrochem. Soc.* 155 (2008) 758–762.
- [30] H. Ishida, *Characterization of Composite Materials*, Butterworth-Heinemann, USA, 1994, pp. 236–238.
- [31] J.D. Ye, S.L. Gu, S.M. Zhu, S.M. Liu, Y.D. Zheng, R. Zhang, Y. Shi, Q. Chen, H.Q. Yu, Y.D. Ye, *Appl. Phys. Lett.* 88 (2006) 101905, 3pp.
- [32] T.L. Phan, R. Vincent, D. Cherns, N.H. Dan, S.C. Yu, *Appl. Phys. Lett.* 93 (2008) 082110, 3pp.
- [33] H.K. Yadav, K. Sreenivas, R.S. Katiyar, V. Gupta, *J. Phys. D: Appl. Phys.* 40 (2007) 6005–6009.
- [34] J. Serrano, A.H. Romero, F.J. Manjón, R. Lauck, M. Cardona, A. Rubio, *Phys. Rev. B* 69 (2004) 094306, 14pp.
- [35] R. Cuscó, E. Alarcón-Lladó, J. Ibáñez, L. Artús, J. Jiménez, B. Wang, M.J. Callahan, *Phys. Rev. B* 75 (2007) 165202, 11pp.
- [36] F. Decremps, J. Pellicer-Porres, A.M. Saitta, J.C. Chervin, A. Polian, *Phys. Rev. B* 65 (2002) 092101, 4pp.
- [37] X. Wang, J. Xu, X. Yu, K. Xue, J. Yu, X. Zhao, *Appl. Phys. Lett.* 91 (2007) 031908, 3pp.
- [38] M.S. Jang, M.K. Ryu, M.H. Yoon, S.H. Lee, H.K. Kim, A. Onodera, S. Kojima, *Curr. Appl. Phys.* 9 (2009) 651–657.
- [39] R. Vinu, G. Madras, *Environ. Sci. Technol.* 42 (2008) 913–919.
- [40] Y.-L. Liao, *Doctoral Thesis*, National Sun Yat-Sen University, 2007.
- [41] V. Subramanian, E.E. Wolf, P.V. Kamat, *J. Phys. Chem. B* 107 (2003) 7479–7485.
- [42] M.A. Fox, M. Dulay, *Chem. Rev.* 93 (1993) 341–357.
- [43] A. Mylonas, E. Papaconstantinou, V. Roussis, *Polyhedron* 15 (1996) 3211–3217.
- [44] E.J. Land, M. Ebert, *Trans. Faraday Soc.* 63 (1967) 1181–1190.
- [45] J. Dzenzel, J. Theurich, D.W. Bahnemann, *Environ. Sci. Technol.* 33 (1999) 294–300.
- [46] L. Zhang, T. Kanki, N. Sano, *Environ. Monit. Assess.* 115 (2006) 395–403.